Original

Herrnring, J.; Kashaev, N.; Klusemann, B.:

Precipitation Kinetics of AA6082: An Experimental and Numerical Investigation

In: Materials Science Forum, THERMEC 2018 (2018) Trans Tech Publications

DOI: 10.4028/www.scientific.net/MSF.941.1411

Materials Science Forum *Online: 2018-12-26*
ISSN: 1662-9752, Vol. 941, pp 1411-1417
doi:10.4028/www.scientific.net/MSF.941.1411

Precipitation Kinetics of AA6082: An Experimental and Numerical Investigation

Jan Herrnring[1,a*], Nikolai Kashaev[1,b] and Benjamin Klusemann[1,2,c]

[1]Institut of Materials Research, Materials Mechanics, Joining and Assessment, Helmholtz-Zentrum Geesthacht, Geesthacht, Germany

[2]Institute of Product and Process Innovation, Leuphana University of Lüneburg, Lüneburg, Germany

[a]Jan.Herrnring@hzg.de, [b]Nikolai.Kashaev@hzg.de, [c]Benjamin.Klusemann@hzg.de

Keywords: Precipitation kinetics, Kampmann-Wagner numerical model, Heat treatment, Laser beam welding, AA6082, simulation.

Abstract. The development of simulation tools for bridging different scales are essential for understanding complex joining processes. For precipitation hardening, the Kampmann-Wagner numerical model (KWN) is an important method to account for non-isothermal second phase precipitation. This model allows to describe nucleation, growth and coarsening of precipitation hardened aluminum alloys based on a size distribution for every phase which produces precipitations. In particular, this work investigates the performance of a KWN model by [1-3] for Al-Mg-Si-alloys. The model is compared against experimental data from isothermal heat treatments taken partially from [2]. Additionally, the model is used for investigation of the precipitation kinetics for a laser beam welding process, illustrating the time-dependent development of the different parameters related to the precipitation kinetics and the resulting yield strength.

Introduction

Since the discovery of precipitation hardening in aluminum alloys at the beginning of the 20th century, aluminum alloys have gained importance and are nowadays one of the most important materials for lightweight structures. Precipitation hardening is by far the most effective way for increasing the mechanical strength of aluminum alloys. Generally the precipitation process consists essentially of three sub-processes, which are nucleation, growth and coarsening [4]. While classical nucleation theories provide the basis for calculation the nucleation rate for stable nuclei, growth describes how already nucleated particles develop under the presence of a concentration gradient. In addition to growth which is decisively driven by diffusion, the coarsening effect is closely related to the Gibbs-Thomson effect [5]. Due to the Gibbs-Thomson effect, larger precipitates growth at the expense of smaller precipitates.

Different simulation approaches are available for solid state precipitation at different scales. Atomistic simulations can be performed via Monte-Carlo methods [6], whereas on the mesoscale the phase field method or Kampmann-Wagner Numerical (KWN) model are well established. KWN models are of particular importance for simulation of second phase precipitation taking into account nucleation, growth and coarsening for systems containing different phases. The majority of works on KWN models assume precipitates as spherical particles, nevertheless few models exists which generalize this approach to non-spherical particles [7, 8]. However, practical implementations strategies of nucleation and growth theories are rare in literature [1, 9]. Following the nomenclature given in [9] an Euler-like multiclass approach is used to describe the precipitation kinetics of the aluminum alloy AA6082 based on a model described in the publications by Myhr and co-workers [1-3]. Their models assume that precipitation kinetics can be efficiently described by only one single particle size distribution, which nucleates and growths as spheres with a stoichiometric chemical composition in the matrix. In the following, the model by Myhr et al.[1-3] is adopted and investigated for isothermal and non-isothermal heat treatments. As specific example for non-

isothermal heat treatments, the model is applied to typical temperature profiles present in laser beam welding.

Microstructure Model

Precipitation Kinetics of 6xxx Series. The resulting mechanical properties of the age hardenable aluminum-magnesium-silicon alloys (6xxx series) depend strongly on the precipitation hardening mechanism. Compared to the influences of precipitation hardening, other hardening effects like the grain size are usually neglected. It is well established that artificial ageing from supersaturated solid solution (SSS) produces a high density of fine hardening precipitates in the aluminum matrix [10]. Best mechanical properties are achieved by metastable precipitates of the fully coherent β''- and the semi-coherent β'-phase. The precipitates efficiently hinder the movement of dislocations in the aluminum matrix. The stable β-phase has generally a negligible influence on mechanical properties. According to [11] the generic precipitation sequence is:

$$SSS \rightarrow Mg\ and\ Si\ Clusters \rightarrow GP\ Zones \rightarrow \beta'' \rightarrow \beta' + [B' + U1 + U2] \rightarrow \beta\ .$$

A common assumption for KWN models of the 6xxx series is to describe the different precipitates by only one phase [12]. For the considered model it is assumed that the phase of the precipitates has the stoichiometric composition Mg_5Si_3 [3]. The diffusion process is described under the usage of the hypothesis of quasi-equilibrium, which means that the composition at the precipitate matrix interface is assumed to have equilibrium composition eventually modified by the Gibbs-Thomson effect.

Evolution Equations of the Microstructure Model. The hardening precipitates in aluminum alloys undergo several, complex and highly coupled effects like nucleation, growth and coarsening. The model by Myhr et al. [1-3], which is adopted in this study, describes the precipitation kinetics by one particle size distribution for spherical particles using a quasi-binary approximation. Nonetheless, more sophisticated KWN models have been proposed in the literature, e.g.[9] which release the quasi-binary approximation. In general, a KWN model based on spheres describes the precipitation kinetics via a particle size distribution $N(r,t)$, which counts the amount of particles in a control volume as a function of time t and radius r. These particles can grow or shrink depending on their radii. Particles larger than a critical radius r^*grow, otherwise they dissolve in the matrix. The velocity of the growth or dissolution process is described by the growth rate v which can be interpreted as a convection term in terms of classic fluid dynamics. The precipitation nucleation process produces continuously new precipitates which are slightly larger than the critical radius r^*. These physical effects can be captured by the following evolution equation for the particle size distribution taken from [1]

$$\frac{\partial \mathrm{N}}{\partial \mathrm{t}} = -\frac{\partial}{\partial \mathrm{r}}[\mathrm{N\ v}] + \mathrm{j}\ \delta(\mathrm{r} - \mathrm{r}^*), \tag{1}$$

using the delta distribution function δ. The constituent elements of the precipitates become tied up and the matrix therefore depletes of those elements during the growth phase. The supersaturation of the constituent elements in the matrix decreases and the system achieves a state that is closer to thermodynamic equilibrium. A mass balance across all size classes determines the mean matrix concentration. A derivation of the mass balance for the general multicomponent case is provided in the recent publication by Du et al. [13]. With the knowledge of the particle volume fraction f_p and the nominal concentration of the alloy c_i^0 as well as the alloy concentration in the precipitate c_i^β, it is possible to obtain the mean concentration of the matrix via [1] as $\mathrm{c}_i^\alpha = \frac{\left[\mathrm{c}_i^0 - \mathrm{f_p c}_i^\beta\right]}{1-\mathrm{f_p}}, i = \{Mg, Si\}$ with $\mathrm{f_p} = \sum_\mathrm{k} \frac{4}{3} \pi\ \mathrm{r}_\mathrm{k}^3\ \mathrm{N_k}$. The nucleation rate j in Eq. (1), describes how many particles nucleate in a unit volume at a distinct time at a given temperature T. According to [1], it can be determined by simplified classic nucleation theory:

$$\mathrm{j} = \mathrm{j}_0 \exp\left(-\left[\frac{\mathrm{A}_0}{\mathrm{RT}}\right]^3 \left[\frac{1}{\ln\left(\mathrm{C}^{\alpha}_{\mathrm{Mg}}/\,\mathrm{C}^{\mathrm{e}}_{\mathrm{Mg}}\right)}\right]^2\right) \exp\left(-\frac{\mathrm{Q_d}}{R\,T}\right). \tag{2}$$

Here denotes j_0 a pre-exponential term, Q_d the activation energy for diffusion, R the gas constant and A_0 a constant that has the same dimension as the activation energy for nucleation. The solution procedure for Eq. (1) is achieved by utilizing standard solution methods of numerical fluid dynamics, in this paper the finite volume method in combination with a linear upwind schema, as outlined in [1], has been applied.

The growth of precipitates is defined using the quasi-binary approximation. A particle is going to growth, if the interface concentration of the matrix $c^{\alpha,i}_{Mg}$, calculated under utilization of the Gibbs-Thomson equation, is exceeded by the concentration of magnesium in the aluminum matrix c^{α}_{Mg}. For a stoichiometric particle with radius r and a current magnesium concentration c^{β}_{Mg}, the growth rate v and critical radius r^* are calculated according to [1] by

$$v = \frac{\mathrm{c}^{\alpha}_{Mg} - \mathrm{c}^{\alpha,i}_{Mg}}{\mathrm{c}^{\beta}_{Mg} - \mathrm{c}^{\alpha,i}_{Mg}} \frac{\mathrm{D}}{\mathrm{r}} \qquad \text{and} \qquad \mathrm{r}^* = \frac{2\sigma \mathrm{V_m}}{\mathrm{RT}} \left[\ln\left(\frac{c^{\alpha}_{Mg}}{c^{\alpha}_{e}}\right)\right]^{-1}. \tag{3}$$

The interface concentration of the matrix $c^{\alpha,i}_{Mg}$ is determined according to [1] by the equilibrium concentration of magnesium in the matrix $\mathrm{c}^{\alpha,\mathrm{e}}_{\mathrm{Mg}}$, the interfacial energy σ and the molar volume of the precipitating phase $\mathrm{V}^{p}_{\mathrm{m}}$ via $\mathrm{c}^{\alpha,i}_{Mg} = \mathrm{c}^{\alpha,\mathrm{e}}_{\mathrm{Mg}} \exp\left(\frac{2\sigma \mathrm{V}^{\mathrm{p}}_{\mathrm{m}}}{\mathrm{r\,R\,T}}\right)$, representing the Gibbs-Thomson effect.

Yield Strength Model. A combined model for work hardening and yield strength corresponding to the microstructure model has been presented in [2, 3, 14]. This model offers the possibility to calculate the yield strength and work hardening caused by dislocations by means of the size distribution function and the equivalent plastic strain. Work hardening is not investigated in this paper, therefore this aspect is not further addressed. The yield strength $\boldsymbol{\sigma_y}$ is additively composed of contributions from the intrinsic yield strength $\boldsymbol{\sigma_i}$, solute solution strengthening $\boldsymbol{\sigma_{ss}}$ and particle strengthening $\boldsymbol{\sigma_p}$ as $\boldsymbol{\sigma_y = \sigma_i + \sigma_{ss} + \sigma_p}$. The contribution from solid solution hardening are calculated by a power law with constant parameters $\mathbf{k_i}$. Taking into account a correction for the effective available silicon content $\mathbf{c^{\alpha}_{Si,eff}}$ in the aluminium matrix, the contribution from solid solution hardening according to [2] is calculated by $\boldsymbol{\sigma_{ss} = k_{Cu}\, c^{\alpha}_{Mg}{}^{\frac{2}{3}} + k_{Si}\, c^{\alpha}_{Si,eff}{}^{\frac{2}{3}} + k_{Cu}\, c^{\alpha}_{Cu}{}^{\frac{2}{3}}}$ with $\boldsymbol{c^{\alpha}_{Si,eff} = c^{\alpha}_{Si} - \frac{1}{3}\left[c^{\alpha}_{0,Fe} + c^{\alpha}_{0,Mn}\right]}$. The contribution of particle hardening is calculated under usage of the Fleischer-Friedel-Point-Obstacle-Approximation [15, 16]. According to this theory the distance in the glide plane depends inversely proportional to the square root of the particle number density in the slip plane. The distance between dislocations decrease under application of shear stresses due to the bending of the dislocation line. Therefore the effective distance between the obstacles decreases, which is accounted by the Friedel-length. The particle strengthening according to [2, 3, 14] is calculated under usage of the Taylor Factor $\mathbf{M}$, mean radius $\bar{\mathbf{r}}$, shear modulus $\mathbf{G}$, Burgers vector $\mathbf{b}$, a constant parameter $\boldsymbol{\beta}$, mean obstacle strength $\bar{\mathbf{F}}$ between obstacle and dislocation line and the total number of particles $\mathbf{N_v}$ as

$$\sigma_{\mathrm{p}} = \frac{\mathrm{M}}{\mathrm{b}^2\sqrt{\mathrm{G}}} \sqrt{\frac{\mathrm{N_v}\,\bar{\mathrm{r}}}{\beta}}\, \bar{F}^{3/2} \qquad \text{with} \qquad \bar{F} = \sum_i \frac{F_i\, N_i}{F_i}. \tag{4}$$

Weak precipitates that are smaller than a critical radius r_c are sheared, otherwise the precipitates are bypassed. The interaction force between dislocation and weak precipitation is calculated by $F_i = 2\beta G b^2 r_i / r_c$, whereas for strong obstacles this force is calculated by $F_i = 2\beta G b^2$. The investigated input parameters for the KWN model and the yield strength model originating from [3], whereby the chemical compositions given in Table 1 determined by a spark spectrometer has been used for simulation.

Table 1: Chemical composition of investigated aluminum alloy 6082 in wt.-%.

Si	Fe	Cu	Mn	Mg	Other	Al
1.195	0.361	0.087	0.444	0.905	0.113	Balance

Experimental and Numerical Study

In Myhr et al. [2] the precipitation model is compared to experimental results for the Vickers hardness HV extracted from [17] under usage of the linear relationship $\sigma_y = 3[MPa]\,HV - 48[MPa]$ for the yield strength for different heat-treatment temperatures. For validation reasons, our implementation results are compared in Fig. 1 to these results. The hardness measurements for 176°C have been performed in this work. Our experimental specimens were solution heat treated at 525°C for 30 minutes. Afterwards, the specimens were quenched in water. Immediately after quenching the samples were heat treated in a salt bath at 176° C and subsequently cold embedded and polished before the hardness tests. The experimental and numerical results show a good agreement to the published experimental and additional to the simulation results from [2] (compare Fig. 9 in [2]). The small differences compared to the simulation results in [2] resulting from the different equilibrium data, taken from [3] and the different alloy composition according to Table 1. Obviously, the decrease of strength during the coarsening regime is predicted with a high degree of accuracy.

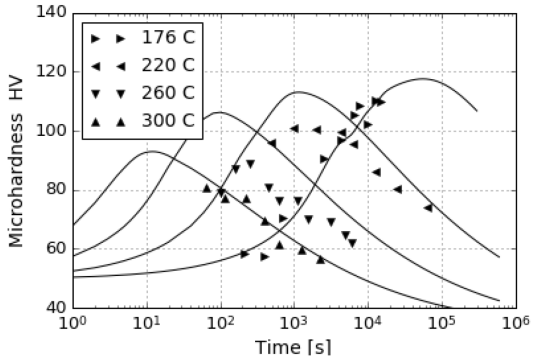

Figure 1: Comparison of simulation results (solid lines) to experimental results (markers) taken from [2] for microhardness results. The experimental values for 176°C were obtained in this work.

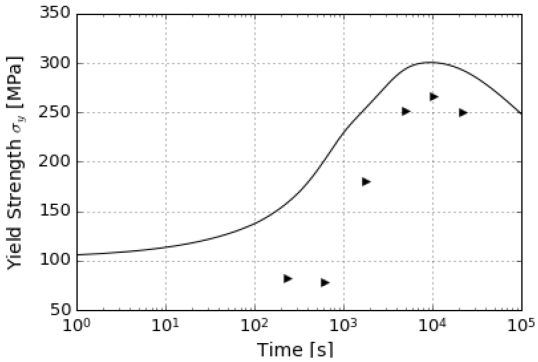

Figure 2: Experimentally measured yield strength (marker) for tensile specimens performing a heat treatment by 193°C and comparison to simulation results (solid line).

Additionally, tensile specimens were prepared accordingly but aged artificially at 193°C in a salt bath. The experimental and numerical results in Fig. 2 show a little bit less agreement. The results of the KWN model delivers higher yield stresses and a faster strengthening compared to the experiments. The considered model shows a significant increase in strength in the early stage of nucleation.

In this regard, it is interesting to investigate the influence of non-isothermal heat treatments. For this purpose a heat transfer model for calculation of temperatures in the heat effected zone for laser beam welding processes of aluminum alloys is used. The results and the location of the investigated Points 1, 2 and 3 are shown in Fig. 3(a). The distance between the adjacent points is 1 mm. The presented temperature evolutions, Fig. 3(a), are calculated via an in house code, which solves the transient, linear heat transfer equation with a moving heat source for a cuboid domain by means of Green's Functions. Fig. 3(b)-(f) illustrates the results of the precipitation hardening model for a peak aged alloy for these temperatures. The increase in temperature leads to a significant decrease in volume fraction of the precipitation phase, Fig. 3(b), the particle number density, Fig. 3(c), as well as the yield strength, Fig. 3(f). The temperature increase leads for all points shortly to a decrease of the mean radius, Fig. 3(d), because the critical radius increases and small precipitates become unstable. During cooling, the point with highest temperatures (P1) shows a short period of

time where a large mean radius but a small nucleation rate is encountered, Fig. 3(e). The following decrease in mean radius results from a decrease of the critical radius in combination with an increase of the nucleation rate. The increase in nucleation rate results in a notable increase of the yield strength for the two highest temperatures, Fig. 3(f), which showed before also the highest strength loss during the temperature increase. The results illustrate the significant loss in strength near the fusion as well as heat affected zone (HAZ). An additional post weld heat treatment could be used to increase the strength in both zones. But this strongly depends on the precipitation conditions. Typically the HAZ does gain significantly less additional strength after the post weld heat treatment due to the large overaged precipitates. This effect is observed in Fig. 3(d) by the strong increase of the mean radius.

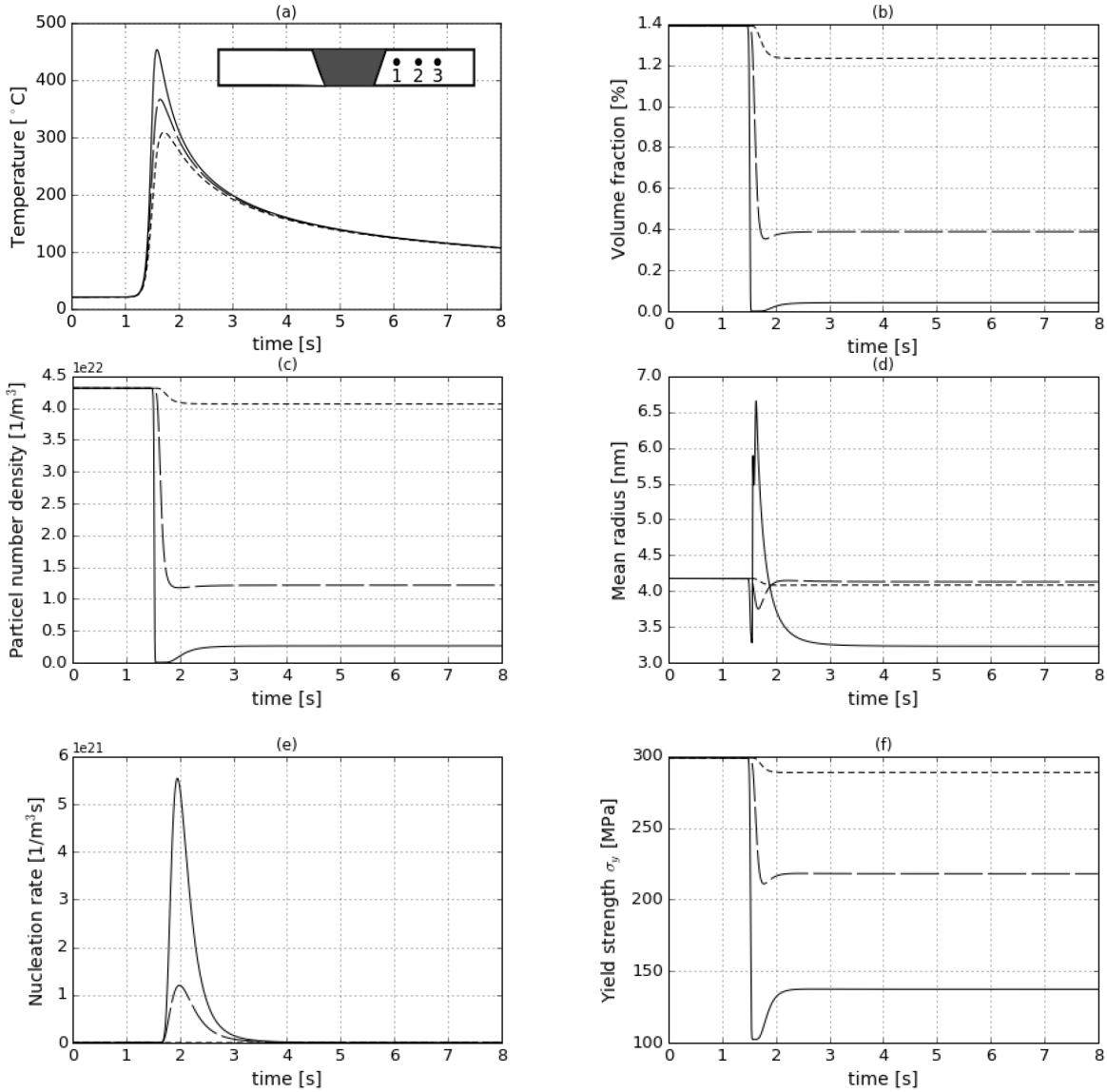

Figure 3: Simulation results for non-isothermal heat treatments following temperatures shown in Fig. 3(a), representative for laser beam welding. The solid line representing Point 1 has a distince of 3 mm to the center of the fusion zone. The distince between the adjacent points is 1 mm (large dashed line – Point 2; small dashed line – Point 3).

Compared to the results in Fig. 1 and Fig. 2 the increase of the yield strength due to a high nucleation rate at 2 seconds shown for Points 1 and 2 in Fig. 3 overestimates the potential of precipitation hardening during cooling. Nucleation and growth or dissolution are sensitive to the used equilibrium data. The considered model describes the precipitation process by one single phase, which is stable up to temperatures next to the solidus temperature. Recent investigations in [18] of the CALPHAD method give a thermodynamic description for further phases like the β''or

β'-phase, which tend to dissolve at much lower temperatures than the β-phase. For more detailed investigations it is necessary to use thermodynamic descriptions for the different phases to give more reliable results over a wide range of temperatures.

Conclusion

A precipitation model for nucleation, growth and coarsening of precipitation hardened aluminum alloys of the 6xxx series, adopted from Myhr et al. [3], has been implemented and investigated for heat treatment and laser beam welding including selected comparisons to experiments. The model gives reasonable results for a wide range of applications and illustrates the core elements of a KWN model. Nevertheless, for increasing the predictive power of the model, more sophisticated approaches for the thermodynamic description, such as the CALPHAD method, are necessary.

References

[1] O. Myhr and Ø. Grong, "Modelling of non-isothermal transformations in alloys containing a particle distribution," Acta Mater., vol. 48, no. 7, pp. 1605-1615, 2000.

[2] O. Myhr, Ø. Grong, and S. Andersen, "Modelling of the age hardening behaviour of Al–Mg–Si alloys," Acta Mater., vol. 49, no. 1, pp. 65-75, 2001.

[3] O. Myhr, Ø. Grong, H. Fjær, and C. Marioara, "Modelling of the microstructure and strength evolution in Al–Mg–Si alloys during multistage thermal processing," Acta Mater., vol. 52, no. 17, pp. 4997-5008, 2004.

[4] R. Wagner, R. Kampmann, and P. W. Voorhees, "Homogeneous Second-Phase Precipitation," in Phase Transformations in Materials: Wiley-VCH, 1991, pp. 310-407.

[5] M. Perez, "Gibbs–Thomson effects in phase transformations," Scr. Mater., vol. 52, no. 8, pp. 709-712, 2005.

[6] P. Binkele and S. Schmauder, "An atomistic Monte Carlo simulation of precipitation in a binary system," Zeitschrift für Metallkunde, vol. 94, no. 8, pp. 858-863, 2003.

[7] B. Holmedal, E. Osmundsen, and Q. Du, "Precipitation of Non-Spherical Particles in Aluminum Alloys Part I: Generalization of the Kampmann–Wagner Numerical Model," Metall. Mater. Trans., vol. 47, no. 1, pp. 581-588, January 01 2016.

[8] Q. Du, B. Holmedal, J. Friis, and C. D. Marioara, "Precipitation of Non-spherical Particles in Aluminum Alloys Part II: Numerical Simulation and Experimental Characterization During Aging Treatment of an Al-Mg-Si Alloy," Metall. Mater. Trans., vol. 47, no. 1, pp. 589-599, January 01 2016.

[9] M. Perez, M. Dumont, and D. Acevedo-Reyes, "Implementation of classical nucleation and growth theories for precipitation," Acta Mater., vol. 56, no. 9, pp. 2119-2132, 2008.

[10] S. Esmaeili, D. Lloyd, and W. Poole, "Modeling of precipitation hardening for the naturally aged Al-Mg-Si-Cu alloy AA6111," Acta Mater., vol. 51, no. 12, pp. 3467-3481, 2003.

[11] A. Falahati, E. Povoden-Karadeniz, P. Lang, P. Warczok, and E. Kozeschnik, "Thermo-kinetic computer simulation of differential scanning calorimetry curves of AlMgSi alloys," Int. J. Mater. Res., vol. 101, no. 9, pp. 1089-1096, 2010.

[12] D. Bardel et al., "Coupled precipitation and yield strength modelling for non-isothermal treatments of a 6061 aluminium alloy," Acta Mater., vol. 62, pp. 129-140, 2014.

[13] Q. Du, K. Tang, C. D. Marioara, S. J. Andersen, B. Holmedal, and R. Holmestad, "Modeling over-ageing in Al-Mg-Si alloys by a multi-phase CALPHAD-coupled Kampmann-Wagner Numerical model," Acta Mater., vol. 122, pp. 178-186, 2017.

[14] O. R. Myhr, Ø. Grong, and K. O. Pedersen, "A combined precipitation, yield strength, and work hardening model for Al-Mg-Si alloys," Metall. Mater. Trans., vol. 41, no. 9, pp. 2276-2289, 2010.

[15] B. Reppich, "Particle strengthening," in Materials Science and Technology: Wiley-VCH, 1993, pp. 311-357.

[16] A. Ardell, "Precipitation hardening," Metall. Mater. Trans., vol. 16, no. 12, pp. 2131-2165, 1985.

[17] W. Anderson, "Precipitation from solid solution," ASM, Metals Park, Ohio, 1959.

[18] E. Povoden-Karadeniz, P. Lang, P. Warczok, A. Falahati, W. Jun, and E. Kozeschnik, "CALPHAD modeling of metastable phases in the Al–Mg–Si system," Calphad, vol. 43, pp. 94-104, 2013.